Electronic Supplementary Material (ESI) for Materials Chemistry Frontiers.
This journal is © the Partner Organisations 2022

Supporting Information

Anchoring MoS_2 on Ethanol-Etched Prussian Blue Analog for Enhanced Electrocatalytic Efficiency for Oxygen Evolution Reaction

Poulami Mukherjee, Krishnamoorthy Sathiyan, Vishwanath R. S and Tomer Zidki*
Department of Chemical Sciences and the Center for Radical Reactions and Materials Research, Ariel University, Ariel, 4077625 Israel.

Electrode preparation. Each catalyst ink for the working-electrode was prepared by dispersing 2.5 mg of sample in a mixture of 200 µL water, 200 µL isopropyl alcohol, and 10 µL of Nafion binder (5 wt% in water/1-propanol mixture) followed by ultrasonication for 15 min. Before using the GCE, the surface was polished with 0.3 µm and 0.05 µm of alumina powder to smooth the surface. It was sonicated in water for 1 min to remove any particles. Later, 30 CV cycles were performed in 0.5 M H_2SO_4 to clean it electrochemically. Finally, 10 µL of the ink (catalyst loading ~0.85 mg cm^{-2}) was drop-casted on the thoroughly cleaned GCE and dried at room temperature. Similarly, 20 µL of the ink was loaded on the carbon cloth (CC) electrode with catalyst loading ~0.24 mg cm^{-2}.

Electrocatalytic performance characterization. The electrochemical experiments consisted of cyclic voltammetry (CV), linear sweep voltammetry (LSV), and electrochemical impedance spectroscopy (EIS) were conducted using the PalmSens4 potentiostat. All the electrochemical measurements were performed with a standard three-electrode cell set-up equipped with GCE (0.071 cm^2) or carbon cloth (2.0 cm^2) electrodes deposited with the prepared OER electrocatalysts as the working-electrode in a 1.0 M KOH electrolyte. A Hg/HgO (1.0 M KOH) and graphite rod were employed as reference and counter electrodes, respectively. Before the electrochemical analysis, the electrolyte solutions were degassed with N_2 for 30 minutes. All the measured potentials were calculated relative to the reversible hydrogen electrode (RHE) using the Nernst equation $E_{(\text{vs. RHE})} = E_{(\text{vs. Hg/HgO})} + 0.098 + 0.059 \times \text{pH}$. The working-electrode geometrical areas were normalized in all the CVs and LSVs to obtain the current densities.

The electrochemical surface area (ECSA) is estimated from the electrochemical double-layer capacitance (C_{dl}) at the catalyst│electrolyte interface. CVs of different scan rates were performed in the non-faradaic region; both capacitive currents (oxidative and reductive) at the middle of the potential window were averaged and plotted against the scan rate to get C_{dl} values. The ECSA values of the catalysts deposited on GCE and CC were calculated by applying a general specific capacitance of 40 μFcm^{-2} (in 1.0 M KOH) based on previous reports.[1–5] EIS experiments (frequency range of 100 kHz to 0.01 Hz with 5 mV amplitude) were performed under the O_2 evolution regime (at 1.6 V vs. RHE). The long-term stability of the catalyst was examined by chronoamperometry (CA) at an applied overpotential of 260 mV vs. RHE (at a current density of 10 mA cm^{-2}) for 24 hours.

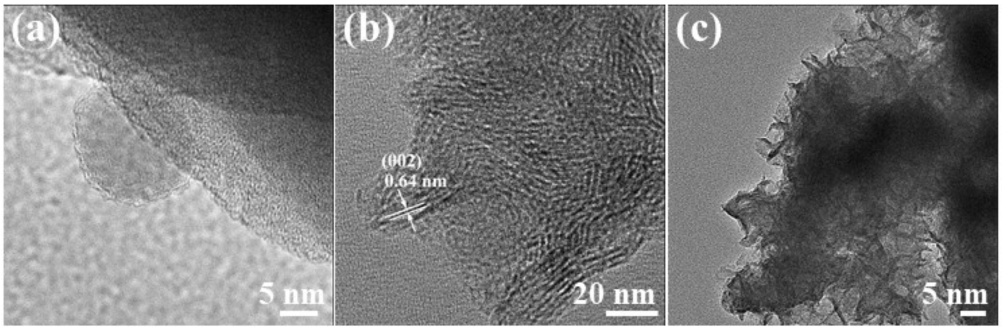

Fig S1. HR-TEM images of **(a)** Etched-PBA, **(b)** MoS_2, and **(c)** TEM image MoS_2.

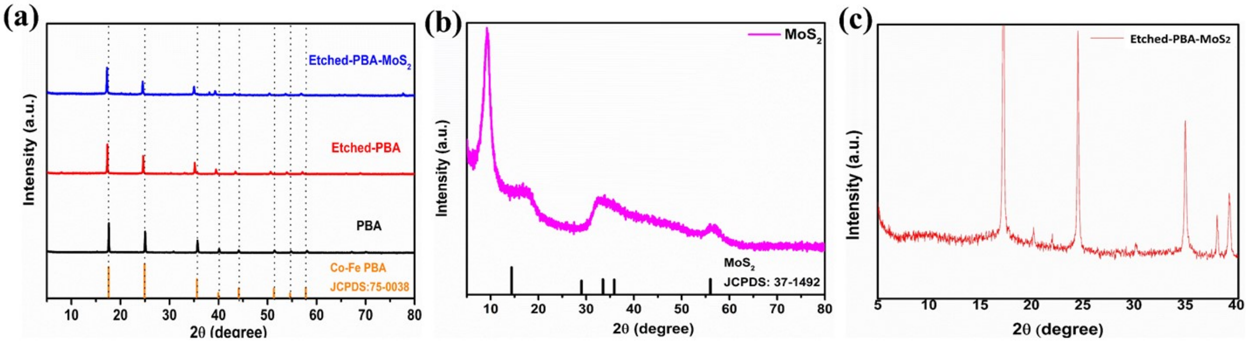

Fig S2. XRD patterns of **(a)** PBA, Etched-PBA, Etched-PBA-MoS_2, **(b)** slow scan of MoS_2, and **(c)** slow scan of Etched-PBA-MoS_2.

Table S1. Elemental mappings of Co, Fe, Mo, and S as determined by EDX analysis.

Sample	Co (at. %)	Fe (at. %)	Mo (at. %)	S (at. %)	Co/Fe
Etched-PBA-MoS_2	38.42	38.41	7.02	16.15	1.00
Etched-PBA	51.15	48.85	-	-	1.04
PBA-MoS_2	45.46	29.76	7.35	15.43	1.52
MoS_2	-	-	33.95	66.05	-
PBA	57.23	42.77	-	-	1.46

Table S2. ICP-OES analysis of the various catalysts.

Sample	Co (at. %)	Fe (at. %)	Mo (at. %)	Co/Fe
Etched-PBA-MoS_2	36.97	58.13	4.90	0.63
Etched-PBA	39.65	60.35	-	0.65
PBA-MoS_2	57.99	37.42	4.68	1.55
MoS_2	-	-	100	-
PBA	62.33	40.67	-	1.53

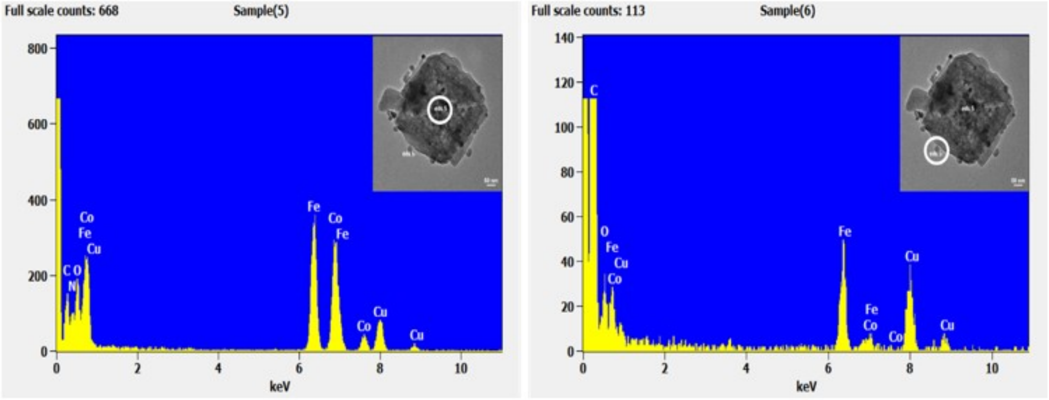

Element	Weight %	Atomic %
Fe	52.85	54.19
Co	47.15	45.81

Element	Weight %	Atomic %
Fe	98.48	98.56
Co	1.52	1.44

Fig S3. EDX spectra of Etched-PBA from the center (left image) and the edge (right image) of the cube.

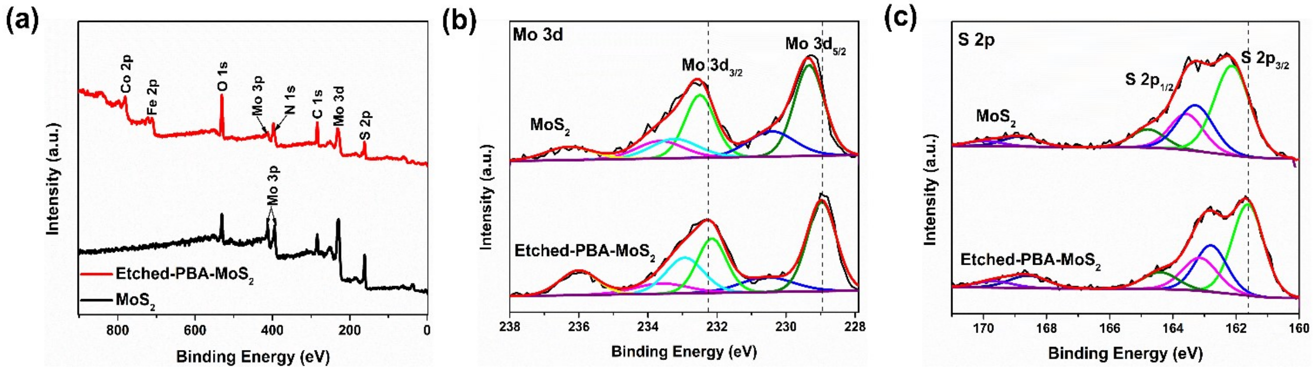

Fig S4. XPS comparison spectra of Etched-PBA-MoS_2 and MoS_2. **(a)** survey spectra; **(b)** high-resolution spectra of Mo 3d; **(c)** high-resolution spectra of S 2p.

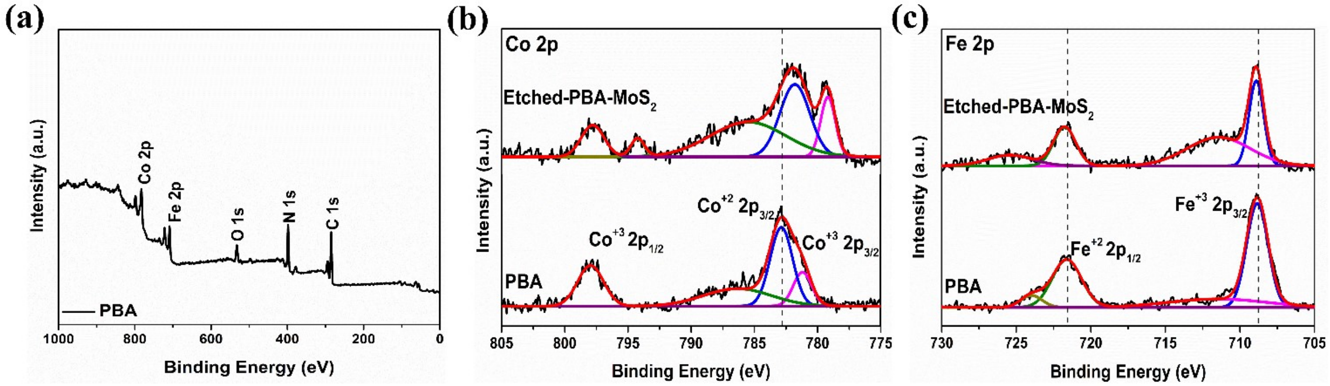

Fig S5. (a) XPS survey spectrum of PBA; **(b)** Comparison high-resolution spectra of Co 2p; **(c)** Fe 2p of Etched-PBA-MoS_2 and PBA.

The BE peaks of PBA at 781.1 and 798.1 eV are ascribed to the Co^{3+} $2p_{3/2}$ and $2p_{1/2,}$ respectively, Fig S5b.[6] The peak at 782.7 eV belongs to Co^{2+} $2p_{3/2}$ spin-orbital.[6] In Etched-PBA-MoS_2, the Co^{3+} $2p_{3/2}$ peak shifts to 779.1 eV, Co^{3+} $2p_{1/2}$ peak to 797.4, and Co^{2+} $2p_{3/2}$ peak to lower BE of 781.8 eV. For Etched-PBA-MoS_2, a new peak at 794.3 eV belongs to the spin-orbitals of Co $2p_{1/2}$, assigned to Co–S.[7] The XPS peaks of Fe^{3+} $2p_{3/2}$ is located at 708.7 eV and Fe^{2+} $2p_{1/2}$ at 721.6 eV for PBA, Fig S5c.[6] The Fe^{3+} peak shifts to 709.1 eV in Etched-PBA-MoS_2, and the Fe^{2+} peak slightly shifts to 721.8 eV. The Fe peak at 712.0 eV that belongs to the Fe^{3+} state in FeOOH (active species) increases in the etching process of Etched-PBA-MoS_2.[8,9] Thus, the Etched-PBA-MoS_2 contains Co^{2+}, Fe^{2+}, Co^{3+}, $Fe^{3+}{}_{,}$ and S^{2-} as expected for bimetallic sulfides.

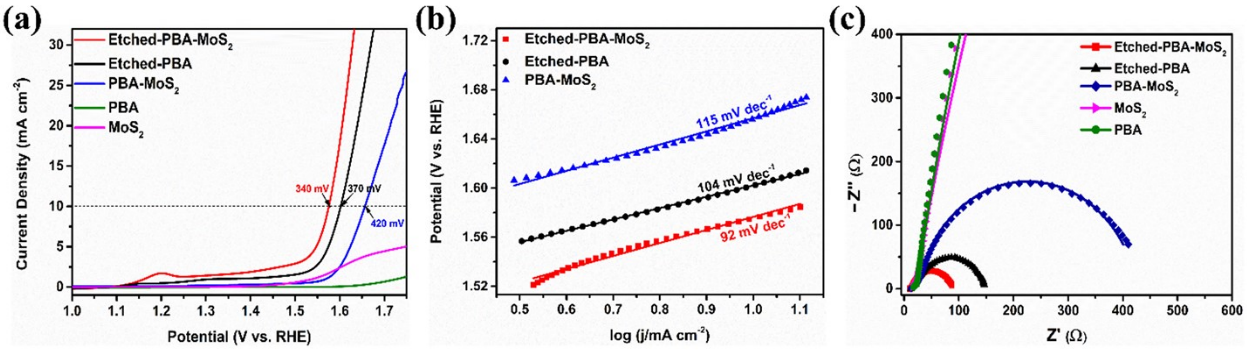

Fig S6. (a) LSV curves of electrocatalysts deposited on GCE at 5 mV s^{-1} in 1.0 M KOH; **(b)** Corresponding Tafel plots; **(c)** EIS-Nyquist plots measured at 1.57 V vs. RHE in 1.0 M KOH.

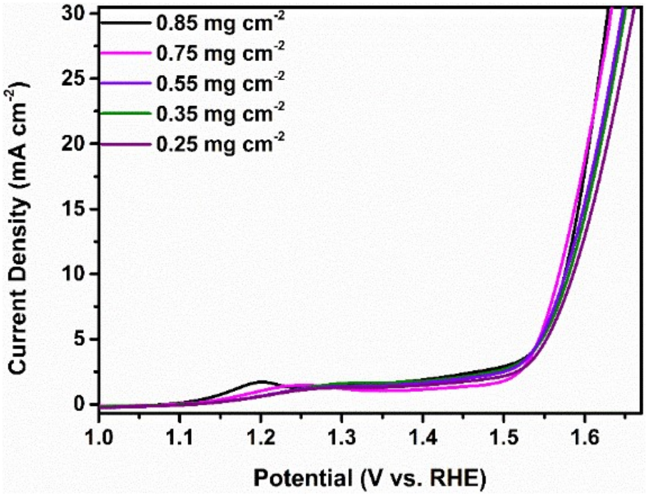

Fig S7. LSVs of Etched-PBA-MoS$_2$ in 1.0 M KOH at 5 mV s^{-1} with different loadings.

We noticed that the 0.85 mg cm^{-2} gives better results, requiring a lower potential to achieve the higher OER current density**.**

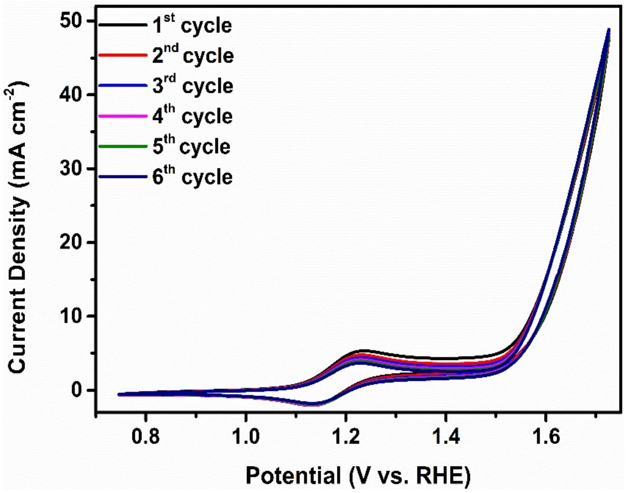

Fig S8. Continuous CVs of Etched-PBA-MoS_2 in 1.0 M KOH at 5 mV s^{-1} on GCE.

Table S3: Summary of Onset potential, Overpotential, and Tafel slope values of all the electrocatalysts deposited on the GCE and CC substrates.

Glassy carbon electrode		
Electrocatalysts	**Overpotential (mV) @10 mA cm^{-2}**	**Tafel slope (mV/dec)**
Etched-PBA-MoS_2	340 mV	92 mV dec^{-1}
Etched-PBA	370 mV	104 mV dec^{-1}
PBA-MoS_2	420 mV	115 mV dec^{-1}

Carbon cloth substrate		
Electrocatalysts	**Overpotential (mV) @ 10 mA cm**	**Tafel slope (mV/dec)**
Etched-PBA-MoS_2	260 mV	55 mV dec^{-1}
Etched-PBA	310 mV	60 mV dec^{-1}
PBA-MoS_2	360 mV	76 mV dec^{-1}

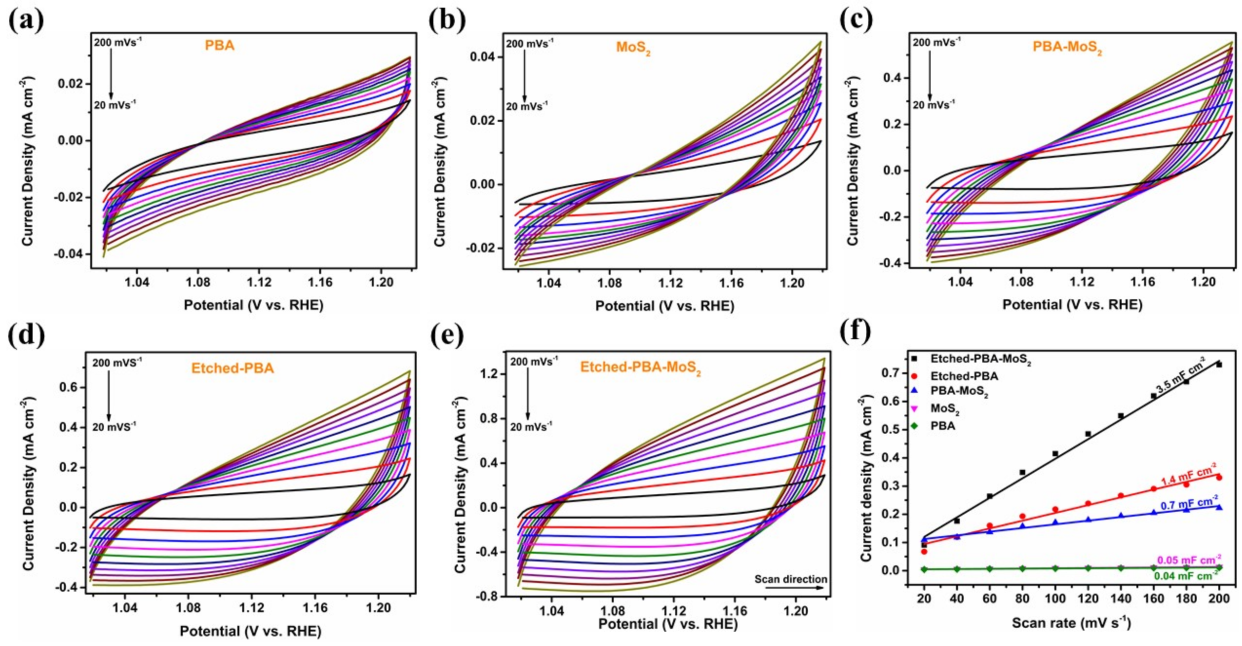

Fig S9. CVs performed at the different scan rates in the non-faradic region for: **(a)** PBA, **(b)** MoS_2, **(c)** PBA-MoS_2, **(d)** Etched-PBA, and **(e)** Etched-PBA-MoS_2 electrocatalysts deposited on GCE and immersed in 1.0 M KOH. **(f)** The plot of the current density differences in the middle of the potential window versus the scan rate.

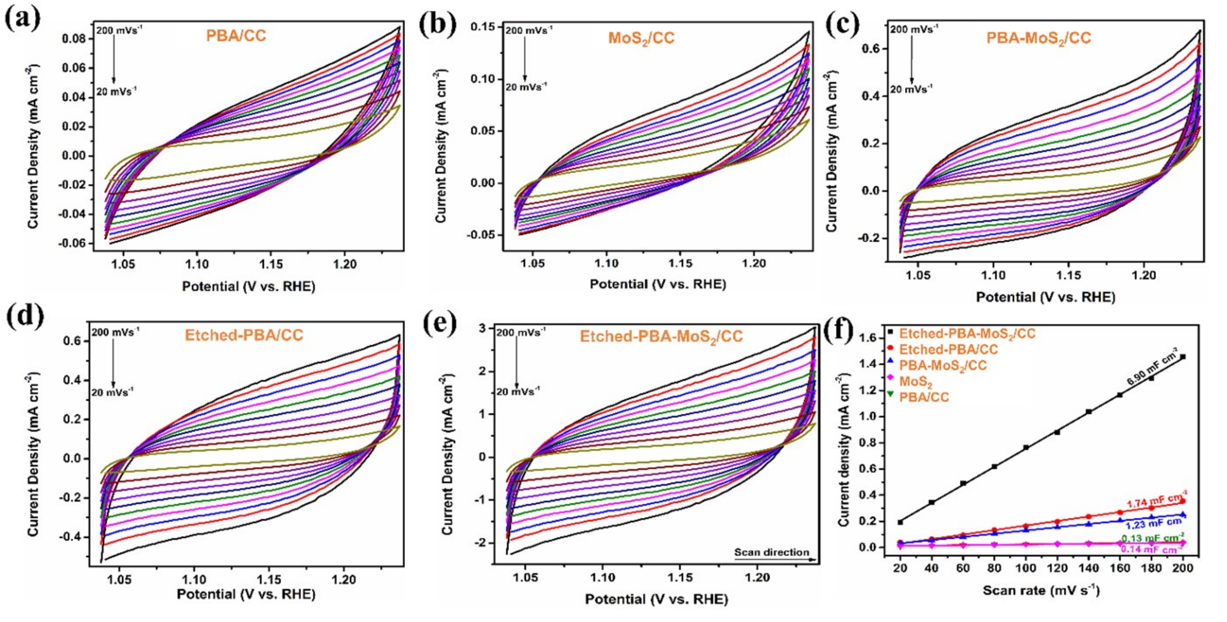

Fig S10. CVs measured at the different scan rates in the non-faradic region for **(a)** PBA, **(b)** MoS_2, **(c)** PBA-MoS_2, **(d)** Etched-PBA, and **(e)** Etched-PBA-MoS_2 electrocatalysts deposited on CC substrate and submerged in 1.0 M KOH. **(f)** The plot of the current density differences in the middle of the potential window versus the scan rate.

Table S4: Summarized double-layer capacitance (C_{dl}) and electrochemical active surface area (ECSA) values of all electrocatalysts deposited on the GCE and CC substrates.

Glassy carbon electrode		
Electrocatalysts	**C_{dl} (mF/cm^2)**	**ECSA (cm^2)**
Etched-PBA-MoS_2	3.5	87.5
Etched-PBA	1.4	35.0
PBA-MoS_2	0.7	17.5
MoS_2	0.05	1.3
PBA	0.04	1.0

Carbon cloth substrate		
Electrocatalysts	**C_{dl} (mF/cm^2)**	**ECSA (cm^2)**
Etched-PBA-MoS_2	6.9	172.5
Etched-PBA	1.74	43.5
PBA-MoS_2	1.23	30.7
MoS_2	0.14	3.5
PBA	0.13	3.3

Note: ECSA values were calculated using the equation: ECSA = Cdl / Cs, where Cs is specific capacitance. We used a general specific capacitance value of 40 μF cm^{-2} (in 1M KOH) based on the previous reports [1–5] to calculate ECSA values of all catalysts deposited on GCE and CC substrates.

Table S5. The fitting results of the impedance electrochemical element parameters of various samples.

Carbon cloth substrate					
Electrocatalysts	**R_s**	**R_{ct}**	**Q_{dl}**	**R_f**	**Q_f**
Etched-PBA-MoS_2	2.614	32.82	0.9494	0.726	0.6887
Etched-PBA	3.213	95.09	0.8577	0.710	0.6270
PBA-MoS_2	2.987	175.4	0.9045	35.252	0.8706
MoS_2	2.477	336.7	0.8813	33.618	0.8089
PBA	3.932	505.1	0.9134	86.983	0.8766

Glassy carbon electrode

Electrocatalysts	**R_s**	**R_{ct}**	**Q_{dl}**	**R_f**	**Q_f**

Etched-PBA-MoS$_2$	10.67	71.34	0.8825	4.178	0.6035
Etched-PBA	10.87	124.8	0.8477	10.975	0.5460
PBA-MoS$_2$	12.32	399	0.8920	14.970	0.5859
MoS$_2$	15.13	1123	0.8811	4.766	0.8774
PBA	17.12	1456	1.0000	4.381	0.8903

R$_s$ is the uncompensated solution resistance in the equivalent circuit; Q$_{dl}$ is the constant phase element (CPE) related to the electrochemical double-layer capacitance at the catalyst│electrolyte interface; **R$_{ct}$** is the charge transfer resistance between the interfaces; **Q$_f$** is the CPE associated with the capacitance of the catalyst thin-film; **R$_f$** is the total resistance at the electrode│catalyst interface and charge transfer within the catalyst film.

Fig S11. HR-SEM images of Etched-PBA-MoS$_2$ (**a-b**) before and (**c-d**) after long-term electrocatalytic OER stability measurements.

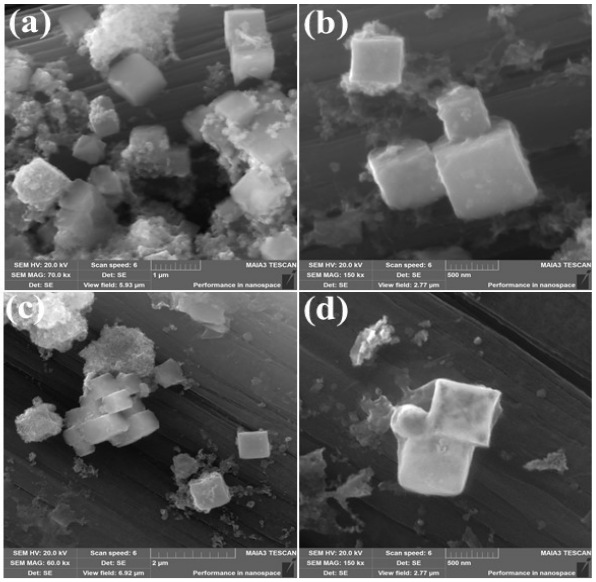

Table S6: Elemental mappings of Co, Fe, Mo, and O as determined by EDX analysis before and after stability.

Etched-PBA-MoS$_2$	**Before Stability**	**After Stability**
Elements	**Atomic %**	**Atomic %**
Co	22.6	11.3
Fe	15.5	8.5
Mo	6.5	3.5
O	55.4	76.7

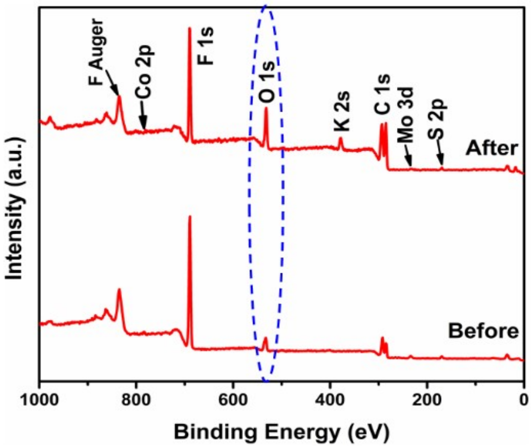

Fig S12. XPS survey spectra of Etched-PBA-MoS_2 before and after stability measurement.
*The catalyst was loaded on the electrode using a Nafion binder, resulting in diminishing the Fe signal and the sharp F peak in both spectra.

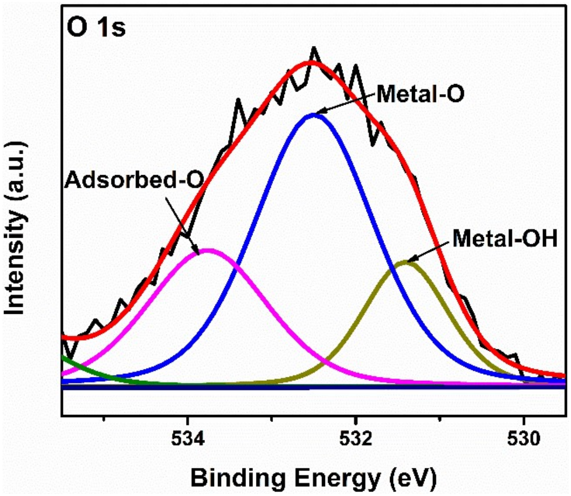

Fig S13. High-resolution XPS spectrum of O1s for Etched-PBA-MoS_2 after stability measurement.

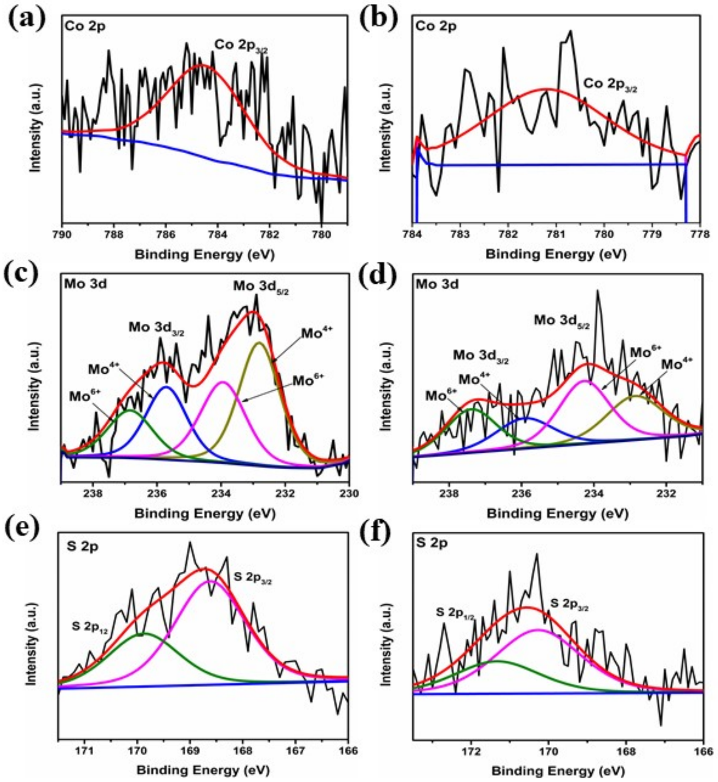

Fig S14. High-resolution XPS spectra of Co 2p (before) **(a)**; Co 2p (after) **(b)**; Mo 3d (before) **(c)**; Mo 3d (after) **(d)**, S 2p (before) **(e)** and S 2p (after) **(f)** stability measurement for Etched-PBA-MoS_2.

Table S7. Composition of Co, Mo, O, and S determined through the XPS quantitative analysis before and after cyclic stability.

Elements	**Before Stability**	**After Stability**	**Before Stability**	**After Stability**
Name	**BE peak (eV)**	**BE peak (eV)**	**Atomic %**	**Atomic %**
Co 2p	784.5	780.8	0.47	0.28
Mo 3d	233.9	234.3	0.58	0.53
S 2p	169.9	170.8	5.22	2.7
O 1s	533.1	532.5	14.51	34.02

Table S8. Comparison of OER catalytic performance of different non-precious-metal-based catalysts.

Catalysts	**Substrate**	**Electrolyte**	**Current density (mA cm^{-2})**	**Overpotential η_{10} (mV)**	**Ref.**
Fe-Co oxides	CC	1M KOH	10	460	10
Co_9S_8@MoS_2	GCE	1 M KOH	10	430	11
MoS_2/Co-N-CN_2-900°C	GCE	1 M KOH	10	442	12
$Fe_{0.5}Ni_{0.5}Co_2O_4$		1 M KOH	10	350	13
MoS_2/CoB-Se/CC	CC	1 M KOH	86	270	14
FeCo oxide	GCE	1 M KOH	10	310	15
$Ni_xCo_{3-X}O_4$	NF	1 M KOH	10	287	16
NiCoS-3 polyhedron	GCE	1 M KOH	10	320	17
MoS_2-decorated NiFe-NCNT	NCNT	1 M KOH	10	370	18
$FeCo_2O_4$	Graphene	0.1 M KOH	10	480	19
Co_3O_4	Cu foil	1 M KOH	10	310	20
CoFe hollow cages(CFHC)	GCE	1 M KOH	10	330	6
$[Co_2(\mu\text{-}Cl)_2(btta)]$	GCE	1 M KOH	10	290	21
$NiCo_{2-x}Fe_xO_4$ nanoboxes	CP	1 M KOH	10	274	22
MoP/NiFeP hybrid hollow spheres		1 M KOH	10	256	23
$CoNi_2S_4$ yolk-shell spheres		1 M KOH	10	282	24
Etched-PBA-MoS_2	**GCE** **CC**	**1 M KOH**	**10**	**340** **260**	**This Work**

References

1 C. C. L. McCrory, S. Jung, J. C. Peters and T. F. Jaramillo, Benchmarking Heterogeneous Electrocatalysts for the Oxygen Evolution Reaction, *J Am Chem Soc*, 2013, **135**, 16977–16987.

2 M. Sadaqat, S. Manzoor, L. Nisar, A. Hassan, D. Tyagi, J. H. Shah, M. N. Ashiq, K. S. Joya, T. Alshahrani and M. Najam-ul-Haq, Iron Doped Nickel Ditelluride Hierarchical Nanoflakes Arrays Directly Grown on Nickel Foam as Robust Electrodes for Oxygen Evolution Reaction, *Electrochim Acta*, 2021, **371**, 137830.

3 A. Roy, K.-M. Kang, Y.-C. Nah, M. La, D. Choi and S. J. Park, Improved Electrocatalytic Water Oxidation with Cobalt Hydroxide Nano-Flakes Supported on Copper-Modified Nickel Foam, *Electrochim Acta*, 2021, **383**, 138368.

4 M. P. Browne, H. Nolan, G. S. Duesberg, P. E. Colavita and M. E. G. Lyons, Low-Overpotential High-Activity Mixed Manganese and Ruthenium Oxide Electrocatalysts for Oxygen Evolution Reaction in Alkaline Media, *ACS Catal*, 2016, **6**, 2408–2415.

5 P. Connor, J. Schuch, B. Kaiser and W. Jaegermann, The Determination of Electrochemical Active Surface Area and Specific Capacity Revisited for the System MnO_x as an Oxygen Evolution Catalyst, *Zeitschrift für Phys Chemie*, 2020, **234**, 979–994.

6 Y. Feng, X. Wang, P. Dong, J. Li, L. Feng, J. Huang, L. Cao, L. Feng, K. Kajiyoshi and C. Wang, Boosting the Activity of Prussian-Blue Analogue as Efficient Electrocatalyst for Water and Urea Oxidation, *Sci Rep*, 2019, **9**, 1–11.

7 Y. Huang, D. Lv, Z. Zhang, Y. Ding, F. Lai, Q. Wu, H. Wang, Q. Li, Y. Cai and Z. Ma, Co-Fe Bimetallic Sulfide with Robust Chemical Adsorption and Catalytic Activity for Polysulfides in Lithium-Sulfur Batteries, *Chem Eng J*, 2020, **387**, 124122.

8 Y. Popat, M. Orlandi, S. Gupta, N. Bazzanella, S. Pillai, M. K. Patel, A. Miotello and N. Patel, Morphological and Elemental Investigations on Co–Fe–B–O Thin Films Deposited by Pulsed Laser Deposition for Alkaline Water Oxidation: Charge Exchange Efficiency as the Prevailing Factor in Comparison with the Adsorption Process, *Catal Letters*, 2022, **152**, 438–451.

9 J. Wu, H. Zheng, F. Zhang, R. J. Zeng and B. Xing, Iron-Carbon Composite from Carbonization of Iron-Crosslinked Sodium Alginate for Cr(VI) Removal, *Chem Eng J*, 2019, **362**, 21–29.

10 M. Ishizaki, H. Fujii, K. Toshima, H. Tanno, H. Sutoh and M. Kurihara, Preparation of

Co-Fe oxides Immobilized on Carbon Paper Using Water-Dispersible Prussian-Blue Analog Nanoparticles and Their Oxygen Evolution Reaction (OER) Catalytic Activities, *Inorganica Chim Acta*, 2020, **502**, 119345.

11 H. Zhu, J. Zhang, R. Yanzhang, M. Du, Q. Wang, G. Gao, J. Wu, G. Wu, M. Zhang, B. Liu, J. Yao and X. Zhang, When Cubic Cobalt Sulfide Meets Layered Molybdenum Disulfide: A Core-Shell System Toward Synergetic Electrocatalytic Water Splitting, *Adv Mater*, 2015, **27**, 4752–4759.

12 X. Hou, H. Zhou, M. Zhao, Y. Cai and Q. Wei, MoS_2 Nanoplates Embedded in Co–N-Doped Carbon Nanocages as Efficient Catalyst for HER and OER, *ACS Sustain Chem Eng*, 2020, **8**, 5724–5733.

13 K.-L. Yan, X. Shang, Z. Li, B. Dong, X. Li, W.-K. Gao, J.-Q. Chi, Y.-M. Chai and C.-G. Liu, Ternary Mixed Metal Fe-Doped $NiCo_2O_4$ Nanowires as Efficient Electrocatalysts for Oxygen Evolution Reaction, *Appl Surf Sci*, 2017, **416**, 371–378.

14 M. Song, Y. Zhao, Z. Wu and X. Liu, MoS_2/CoB with Se Doping on Carbon Cloth to Drive Overall Water-Splitting in an Alkaline Electrolyte, *Sustain Energy Fuels*, 2020, **4**, 5036–5041.

15 C.-H. Chuang, L.-Y. Hsiao, M.-H. Yeh, Y.-C. Wang, S.-C. Chang, L.-D. Tsai and K.-C. Ho, Prussian Blue Analogue-Derived Metal Oxides as Electrocatalysts for Oxygen Evolution Reaction: Tailoring the Molar Ratio of Cobalt to Iron, *ACS Appl Energy Mater*, 2020, **3**, 11752–11762.

16 Y. Shen, S.-G. Guo, F. Du, X.-B. Yuan, Y. Zhang, J. Hu, Q. Shen, W. Luo, A. Alsaedi, T. Hayat, G. Wen, G.-L. Li, Y. Zhou and Z. Zou, Prussian Blue Analogue-Derived Ni and Co Bimetallic Oxide Nanoplate Arrays Block-Built from Porous and Hollow Nanocubes for the Efficient Oxygen Evolution Reaction, *Nanoscale*, 2019, **11**, 11765–11773.

17 Z. Yu, Y. Bai, S. Zhang, Y. Liu, N. Zhang and K. Sun, MOF-Directed Templating Synthesis of Hollow Nickel-Cobalt Sulfide with Enhanced Electrocatalytic Activity for Oxygen Evolution, *Int J Hydrogen Energy*, 2018, **43**, 8815–8823.

18 T. Wang, X. Zhang, P. Yang and S. P. Jiang, Vertically Aligned MoS_2 Nanosheets on N-Doped Carbon Nanotubes with NiFe Alloy for Overall Water Splitting, *Inorg Chem Front*, 2020, **7**, 3578–3587.

19 W. Yan, Z. Yang, W. Bian and R. Yang, $FeCo_2O_4$/Hollow Graphene Spheres Hybrid with

Enhanced Electrocatalytic Activities for Oxygen Reduction and Oxygen Evolution Reaction, *Carbon*, 2015, **92**, 74–83.

20 T. Y. Ma, S. Dai, M. Jaroniec and S. Z. Qiao, Metal–Organic Framework Derived Hybrid Co_3O_4 -Carbon Porous Nanowire Arrays as Reversible Oxygen Evolution Electrodes, *J Am Chem Soc*, 2014, **136**, 13925–13931.

21 X.-F. Lu, P.-Q. Liao, J.-W. Wang, J.-X. Wu, X.-W. Chen, C.-T. He, J.-P. Zhang, G.-R. Li and X.-M. Chen, An Alkaline-Stable, Metal Hydroxide Mimicking Metal–Organic Framework for Efficient Electrocatalytic Oxygen Evolution, *J Am Chem Soc*, 2016, **138**, 8336–8339.

22 Y. Huang, S. L. Zhang, X. F. Lu, Z. Wu, D. Luan and X. W. (David) Lou, Trimetallic Spinel $NiCo_{2-x}Fe_xO_4$ Nanoboxes for Highly Efficient Electrocatalytic Oxygen Evolution, *Angew Chemie Int Ed*, 2021, **60**, 11841–11846.

23 L. Lin, M. Chen and L. Wu, Hierarchical MoP/NiFeP Hybrid Hollow Spheres as Highly Efficient Bifunctional Electrocatalysts for Overall Water Splitting, *Mater Chem Front*, 2021, **5**, 375–385.

24 X. F. Lu, S. L. Zhang, W. L. Sim, S. Gao and X. W. (David) Lou, Phosphorized $CoNi_2S_4$ Yolk-Shell Spheres for Highly Efficient Hydrogen Production via Water and Urea Electrolysis, *Angew Chemie Int Ed*, 2021, **60**, 22885–22891.